Acta Geotechnica (2020) 15:17–27
https://doi.org/10.1007/s11440-019-00899-3

RESEARCH PAPER

Impact of bacteria and urease concentration on precipitation kinetics and crystal morphology of calcium carbonate

Kejun Wen[1] · Yang Li[1] · Farshad Amini[1] · Lin Li[2]

Received: 8 May 2019 / Accepted: 25 November 2019 / Published online: 20 December 2019

Abstract
Microbial/Enzyme-induced carbonate precipitation uses bacteria/urease to drive the biogeochemical reactions to generate $CaCO_3$ precipitation. The goal of this study was to assess the impact of initial concentrations of urease and bacteria on precipitation kinetics and crystal morphology (crystal shape and chemical composition) of calcium carbonate precipitation. Experimental results showed that the $CaCO_3$ precipitation kinetics were well-fitted by a modified exponential logistic model with a confidence value of 95%, and higher concentrations of bacteria and urease could increase the precipitation rate of $CaCO_3$. The results of XRD, FTIR and SEM indicated that vaterite phase was the dominant form of $CaCO_3$ crystals in bacteria-induced system, and calcite phase was the primary form of the $CaCO_3$ crystals in urease-induced system. The results also showed that the effect of initial concentrations of bacteria and urease on the morphology of $CaCO_3$ crystals was insignificant.

Keywords Bacteria · $CaCO_3$ precipitation · Crystal morphology · Enzyme-induced carbonate precipitation (EICP) · Kinetics · Microbial-induced carbonate precipitation (MICP) · Urease

1 Introduction

Microbial/Enzyme-induced carbonate precipitation (MICP/EICP) has recently gained much attention from geotechnical engineering researchers for soil improvement [5, 7–9, 14, 30]. MICP utilizes microbes which can produce urease to induce carbonate precipitation, while EICP uses urease directly. In both MICP/EICP processes, urea is hydrolyzed to form ammonium and carbonate ions, and then the Ca^{2+} ions will react with carbonate ions to form calcium carbonate precipitation [17, 18, 22]. The calcium carbonate precipitation can bond the sand partials together to improve the mechanical properties of MICP/EICP-treated soil [3, 6, 10, 19, 29].

✉ Lin Li
lli1@tnstate.edu

[1] Department of Civil and Environmental Engineering, Jackson State University, Jackson, MS 39217, USA

[2] Department of Civil and Architectural Engineering, Tennessee State University, Nashville, TN 37209, USA

There are six $CaCO_3$ mineral polymorphs including calcite, aragonite, vaterite, $CaCO_3$ monohydrate, $CaCO_3$ hexahydrate and amorphous $CaCO_3$ [15, 21, 32]. Many environmental factors including the concentration of Ca^{2+}, pH, temperature and curing time can affect the formation and morphology of $CaCO_3$ crystals [15, 16]. Li et al. [15] studied the calcium carbonate precipitation and crystal morphology induced by microbial carbonic anhydrase. Their results showed that the dominant $CaCO_3$ crystal phase was calcite and the shape of $CaCO_3$ crystal is mainly cubic and polyhedral. Li et al. [16] reported the effect of different initial Ca^{2+} concentrations on the morphology of calcium carbonate precipitation. Their results showed that this biochemical processes produced a mixture of two forms of calcium carbonate precipitation (calcite and vaterite).

Three different morphology of $CaCO_3$ crystals including calcite, aragonite and vaterite has been reported in MICP/EICP [1, 2, 4, 12, 28, 35, 36]. Studies have reported the effects of temperature, bacterial concentration, $CaCl_2$ concentration and Mg^{2+} ions on the precipitation rate and polymorph of MICP process [1, 12]. Wang et al. [28] confirmed that the shape and size of the $CaCO_3$ precipitates

change during the MICP process. Al Qabany et al. [2] investigated the effect of different chemical concentration on $CaCO_3$ crystal pattern in MICP process. They found that the 0.25 M cementation media could result in a uniform distribution of small size calcite, while 0.50 M cementation media achieved more randomly distributed and larger size crystals. Although no quantitative measurement of engineering properties was conducted in their study, they believed that the different crystal patterns could affect the strength and stiffness of the sample. Almajed et al. [3] employed powdered milk to EICP treatment and found that the $CaCO_3$ precipitation crystal (calcite) is larger and mainly focus at inter-particle contents. This crystal pattern significantly contributes to the strength improvement. Zhao et al. [36] investigated the mechanical behaviors of MICP and EICP-treated sand and found that the unconfined compression strength (UCS) of MICP and EICP-treated soil increased with cementation media concentration and reaction time. They also observed that $CaCO_3$ crystal was mainly irregular bulk with around 100 μm in size, and the process catalyzed by bacteria was much more effective than that by urease in terms of engineering soil properties improvement. However, the difference of $CaCO_3$ crystal morphology in MICP and EICP was not investigated in their study. Cheng et al. [7] reported that the mechanical behaviors of MICP-treated sand were influenced by different environmental conditions. They found that higher urease activity of *Bacillus* sp. could result in higher $CaCO_3$ content, but the lower urease activity could contribute to obtaining an effective $CaCO_3$ bonding for treated sand. Low urease activity could generate larger clusters of a size of approximately 20–50 μm which was nearly ten times bigger than that in high urease activity. The different calcium carbonate crystal morphology could affect particle-bond failure mechanism in the form of either a particle-bond interface mode of failure or internal failure of the carbonate crystal along a suture [11].

According to these studies, it has been indicated that the calcium carbonate crystal morphology can be diverse and the mechanical properties and failure mechanisms of MICP/EICP-treated soil could be different at various environmental factors. Very limited information is available on comparing the morphology of calcium carbonate between MICP and EICP, and the morphology mechanisms of the calcium carbonate are still sparse for both MICP and EICP. The precipitation kinetics of $CaCO_3$ crystals and the change of $CaCO_3$ morphology during the MICP/EICP treatment are still unknown. The objective of this paper was to investigate the mechanisms of $CaCO_3$ crystal morphology during MICP/EICP processes at different bacteria and urease concentrations.

2 Materials and methods

2.1 Bacteria and urease

The bacterium used in this study was *Sporosarcina pasteurii* (ATCC 11859). The bacteria is the most popular used in MICP, and the urease enzymes can hydrolyze the urea and produce ammonium, bicarbonate and an increase in the proximal pH, which induces calcium and carbonate to precipitate [10]. Bacterial cell concentration was controlled by measuring absorbance (optical density) of the suspension using a spectrophotometer at 600 nm wavelength, and the measured value is OD_{600}. An Ammonium-Yeast Extract media (ATCC 1376) was used to grow the bacteria cultures to the desired population density. The growth media contained the following per liter of deionized water: 0.13 M Tris buffer (pH = 9.0), 10 g $(NH_4)_2SO_4$ and 20 g yeast extract. Individual components were autoclaved separately and mixed together post-sterilization. The mixture is then autoclaved to prevent contamination. The bacteria were cultivated in culture medium for 40 h at 30 °C. The bacteria solution was centrifuged at 4000 rpm for 20 min, and the supernatant was removed and replaced by fresh culture media. The bacteria solutions were stored in the centrifuge tubes in a refrigerator under the temperature of 4 °C.

The enzyme used in EICP was urease manufactured by ACROS Organics. According to target concentration, certain amount of urease powder was weighted and mixed with deionized water. The solution was mixed for 30 min. This urease solution was used immediately after it was mixed. The use of urease can skip bacteria culture step and reduce the impact of external environmental conditions on bacteria division or growth [14, 33, 36].

2.2 Cementation media

Cementation media was used to provide chemicals to induce calcium carbonate precipitation during the treatment. The cementation medium used in this research was 0.25 M Ca^{2+} which included urea (15 g/L, 0.25 M), $CaCl_2{\cdot}2H_2O$ (36.8 g/L, 0.25 M), NH_4Cl (10 g/L, 0.19 M), $NaHCO_3$ (2.12 g/L, 0.025 M) and nutrient broth (3 g/L).

2.3 Precipitation experiments

Four different bacteria concentrations (OD_{600} = 0.1, 0.3, 0.6 and 1.0) and initial urease concentrations (1.0, 2.5, 5.0 and 8.0 g/L) were set up in this experiment. The four urease concentrations were selected, because the urease activity and electronic conductivity (EC) are similar to those different bacteria concentrations [36]. The

Table 1 Summarized groups list in precipitation experiments

Group ID	Components
Group 1	OD_{600} = 0.1 and urease = 1.0 g/L
Group 2	OD_{600} = 0.3 and urease = 2.5 g/L
Group 3	OD_{600} = 0.6 and urease = 5.0 g/L
Group 4	OD_{600} = 1.0 and urease = 8.0 g/L

experimental group list used in this study is summarized in Table 1. The precipitation experiments were carried out at 25 °C in beakers, and no soil was involved in this experiment. The bacteria or urease solution (5 mL) was extracted by pipette and mixed with cementation media (100 mL). Four glass slices were placed at the bottom of each beaker to collect the precipitations during the MICP/EICP process. A set of time-series experiments was conducted for each mixed solution. The mixed solutions were monitored at 12, 24, 72 and 168 h, and one piece of glass slices was then collected at each time for further SEM analysis.

Another group of experiments was conducted in beaker only. The bacteria or urease solution (5 mL) was extracted by pipette and mixed with cementation media (100 mL). At sampling periods of 12, 24, 48, 72, 96 and 168 h, a 10 mL solution was sampled and filtered. The filtered solution was analyzed for Ca^{2+} concentration. The calcium carbonate precipitation deposited on the bottom of each beaker at different periods was collected for further XRD and FTIR analysis.

The calcium carbonate precipitations on sand particles were also investigated in this study. Ottawa silica sand (99.7% quartz) was used, and the soil sample was prepared by full contact flexible mold, which was developed by Zhao et al. [36]. The sand is uniformly graded with a median particle size of 0.46 mm, and no fines were included. It was classified as poorly graded sand based on the Unified Soil Classification System. The 140 ± 5 g sand was uniformly mixed with 45 mL bacteria or urease solution and then air-pluviated into the mold to reach a median dense condition (dry density of sand ranged from 1.58 to 1.64 g/cm^3). Then, the soil specimens were immerged into the cementation media (Sect. 2.2) and treated for 168 h. The batch reactor is shown in Fig. 1. The soil samples are 1.5 in. (38.1 mm) in diameter and 3.0 in. (76.2 mm) in height. After the reaction, the samples were removed for SEM analysis. All samples were conducted at least in triplicate.

2.4 Analytical procedures

The Ca^{2+} concentration was measured by inductively coupled plasma-optical emission spectrometer (ICP-OES, SHIMADZU). The detect limitation of ICP-OES is one part per billion (ppb). The crystal morphologies of calcium carbonate were determined by Fourier-transform infrared spectroscopy (FTIR, Spectrum Two, PerkinElmer), X-ray diffraction (XRD, MiniFlex 600, Rigaku) and scanning electron microscopy (SEM, Lyra 3, TESCAN Inc). The FTIR spectra were obtained for 50 scans at a resolution of 4 cm^{-1}. The XRD spectra were performed using a Cu target, and the scan was obtained at the exploration range 2θ = 20°–70° and a scanning velocity of 0.15 s/step. The precipitations were mounted on the stubs with adhesive carbon conductive tabs for SEM observation. The prepared SEM samples were imaged by secondary electron detection.

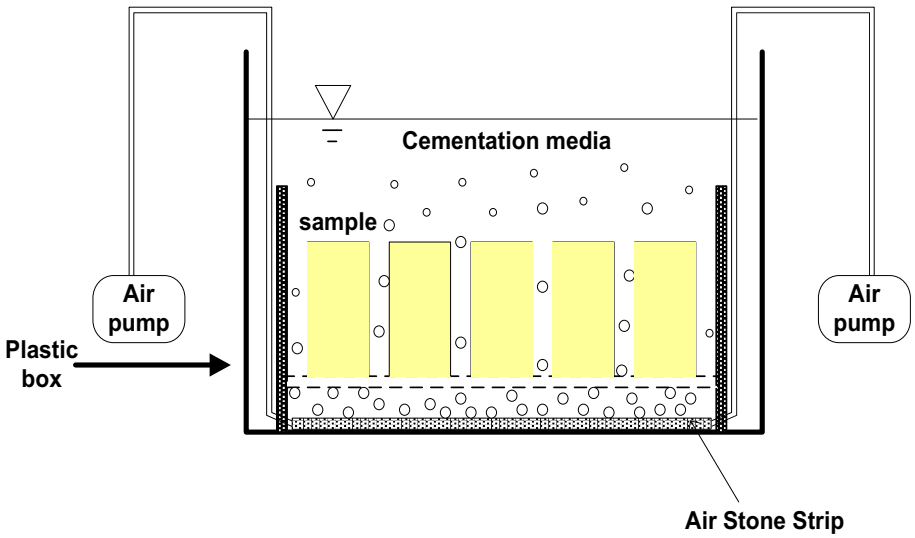

Fig. 1 Batch reactor and setup for immersing treatment

3 Results

3.1 Effects of bacteria and urease concentration on the kinetics of $CaCO_3$ precipitation

Calcium carbonate precipitation can be affected by many external environmental factors, among them the bacteria/urease concentration may be one of the most important factors [2, 23, 36]. The time-dependent behaviors of Ca^{2+} concentration in the mixed solution at different initial concentrations of bacteria and urease are shown in Fig. 2. In the case of group 1 and 2, the Ca^{2+} concentration decreased faster in the urease-induced system in the first 72 h than that in the bacteria-induced system. The Ca^{2+} concentration remained approximately 110 and 100 mmol/L at the end of 72 h in group 1 and 2, respectively, indicating an incomplete reaction in the two groups. The faster decrease in Ca^{2+} concentration in the urease-induced system became more apparent in group 3 and 4. The Ca^{2+} concentration had been completely precipitated in the urease-induced system (8 g/L) of group 4, which was approximately 72 h earlier than that in the bacteria-induced system (OD_{600} = 1.0). It was also clearly seen that the higher initial concentrations of bacteria and urease could yield the faster decreases in Ca^{2+} concentration, which indicated that more $CaCO_3$ precipitations could be generated. However, the high concentration of bacteria and urease concentration does not represent the high urease activity. This conclusion is only correct for this study under the given experimental conditions. Meanwhile, the concentration of Ca^{2+} remained constant or decreased marginally in urease solution after 72 h, which suggested that urease used could be degraded by the surrounding chemicals. In contrast, the Ca^{2+} concentration decreased gradually along with time in the bacteria-induced system. This conclusion is only correct for the cases with lower urease/bacteria concentrations.

The modified exponential logistic model was used to fit the data of precipitated Ca^{2+} concentration according to Stocks-Fischer et al. [25], which expressed as the following regression equation:

$$y_t = \frac{C}{1 + e^{-k(t-t_0)}} \tag{1}$$

where y_t is the amount of precipitated $CaCO_3$, C is the range of y_t (precipitated $CaCO_3$) variation, k is reaction rate

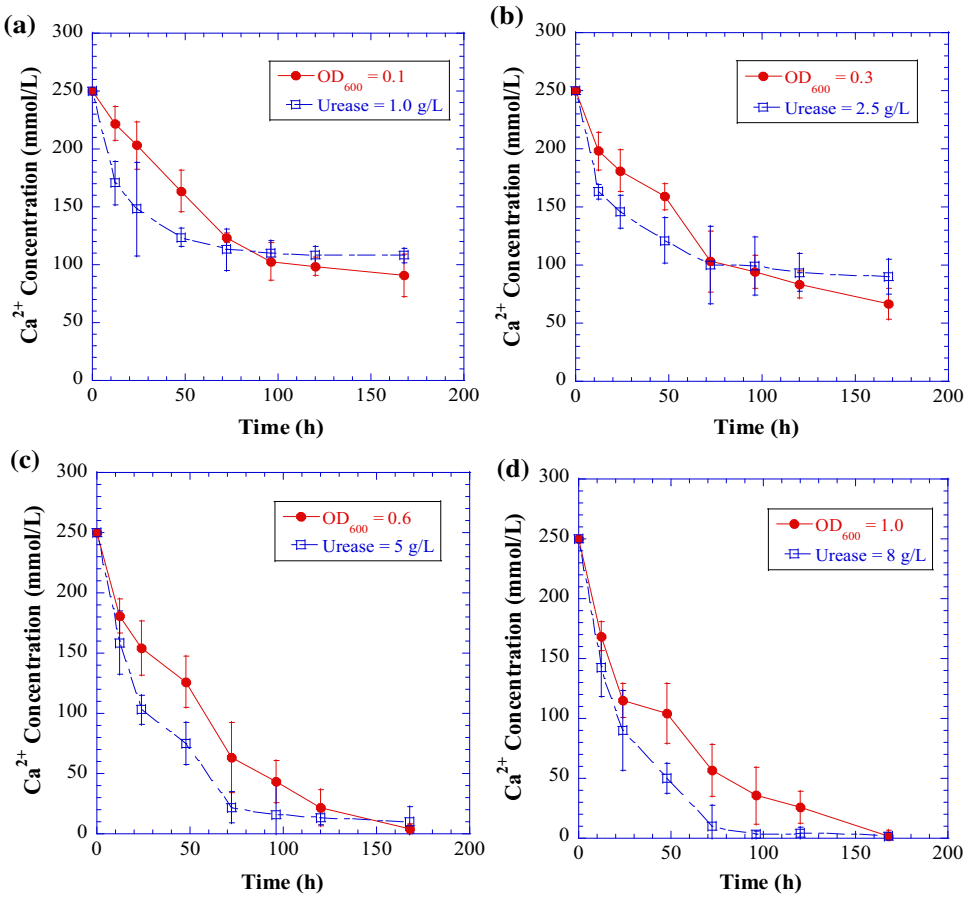

Fig. 2 Temporal Ca^{2+} concentration in the mixed solution at different groups. **a** group 1, **b** group 2, **c** group 3 and **d** group 4

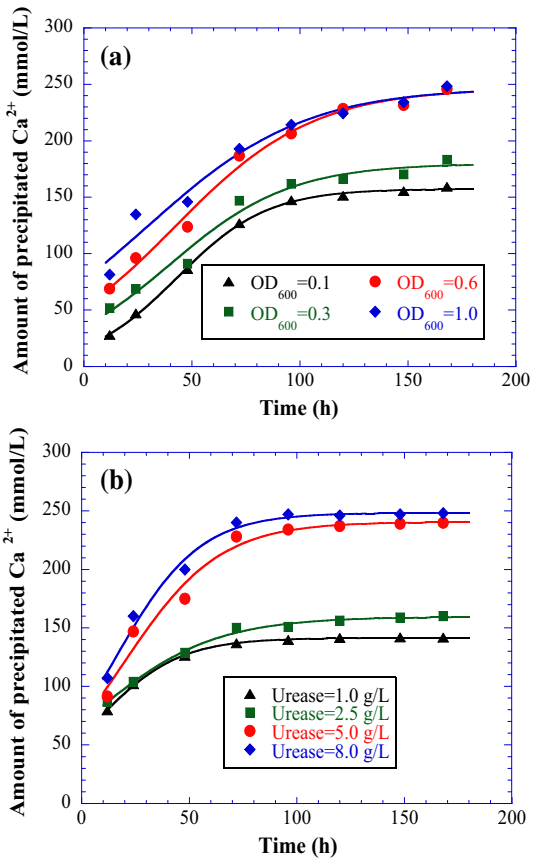

Fig. 3 Exponential logistic model fitting curves of precipitated Ca^{2+} concentration at different initial **a** bacteria concentrations and **b** urease concentrations

constant, t is the reaction time, and t_0 is the time at the maximum (dc/dt). The consumption of Ca^{2+} in MICP/EICP is caused by $CaCO_3$ precipitation. The precipitated Ca^{2+} concentration was calculated by initial Ca^{2+} concentration 250 mmol/L minus Ca^{2+} concentration in the solution. Figure 3 shows the fitting curves at different initial concentrations of bacteria and urease. The model was well-fitted with a confidence value of 95%. Each experiment data point on this graph was the average of at least triplicate samples. Table 2 summarizes equation parameters including C, k, t, t_0. In general, higher initial concentrations of bacteria and urease had a greater rate constant, indicating a faster reaction rate. Moreover, the precipitated Ca^{2+} concentration had only slightly increased or remained constant in urease solution after 72 h. This result is consistent with the finding of the remaining Ca^{2+} concentration in Fig. 2. Stocks-Fischer et al. [25] found that the kinetics of bacteria (sporosarcina pasteurii)-induced $CaCO_3$ precipitations at different initial Ca^{2+} concentration was well-fitted by this model.

3.2 Effects of bacteria and urease concentration on the morphology of $CaCO_3$ crystals

Figure 4 shows the XRD patterns of $CaCO_3$ crystals at the end of each precipitation experiments (168 h). Calcite phase was found in all XRD results, and the leading crystal face of calcite was C(104). An apparent vaterite phase was

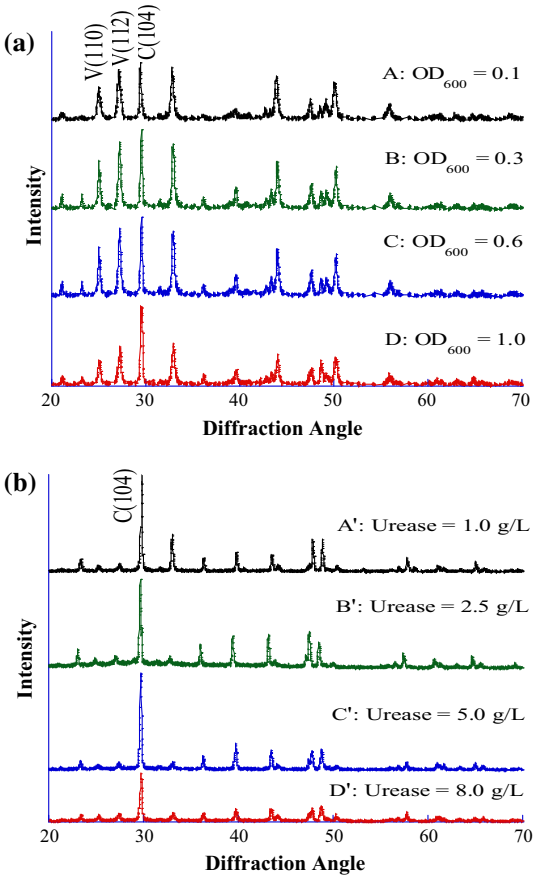

Fig. 4 XRD patterns of $CaCO_3$ crystals at different initial **a** bacteria concentrations and **b** urease concentrations at 168 h

Table 2 Regression parameters of precipitated Ca^{2+} concentration at different initial bacteria and urease concentrations

Bacteria concentration	C (mmol/L)	k (h^{-1})	t_0 (h)	R^2	Urease concentration (g/L)	C (mmol/L)	k (h^{-1})	t_0 (h)	R^2
OD_{600} = 0.1	157.55	0.027	43.09	0.99	1.0	141.60	0.037	6.83	0.99
OD_{600} = 0.3	179.95	0.031	41.56	0.98	2.5	159.56	0.045	7.06	0.99
OD_{600} = 0.6	246.45	0.036	39.38	0.99	5.0	240.53	0.052	15.63	0.97
OD_{600} = 1.0	247.46	0.048	29.56	0.96	8.0	248.36	0.053	19.46	0.98

observed simultaneously in $CaCO_3$ crystals induced by different bacteria concentrations. The diffraction peaks happened at the diffraction angle of 24.9° and 27.1°, respectively, correspond to vaterite face V(110) and V(112). It suggested that urease-induced $CaCO_3$ crystals favored the calcite phase, and bacteria-induced $CaCO_3$ crystals favored the formation of vaterite. The concentration of bacteria or urease did not have an apparent effect on the morphology of $CaCO_3$ crystals.

In order to better understand the formation processes of $CaCO_3$ crystals in the precipitation experiment, the $CaCO_3$ crystals obtained at different precipitation periods were used to conduct FTIR and SEM analysis. The FTIR spectra of $CaCO_3$ crystals at different times in bacteria and urease system are shown in Figs. 5 and 6, respectively. There were no hydrated phases in all systems identified by FTIR absorption bands, because of the absence of absorption bands at 866 and 1074 cm^{-1} [11, 16, 32]. The presence of vaterite and calcite was confirmed by the observation of absorption bands at 747 and 1085 cm^{-1} for vaterite and 711 cm^{-1} for calcite. These similar absorption bands of vaterite (747 and 1085/1084 cm^{-1}) and calcite (708/712 cm^{-1}) were also reported by Loste et al. [20] and Li et al. [16]. There was only vaterite phase existed before 72 h in all bacteria concentration systems. The characteristic absorption band at 711 cm^{-1} was first observed at 120 h as OD_{600} = 0.1 and 1.0, indicating that the calcite phase began to form in the bacteria solution. The calcite phase was formed in all bacteria concentrations at 168 h. This finding was consistent with the results of XRD pattern in the bacteria-induced system. In contrast, the calcite phase was observed in the urease-induced system from the beginning 12 h. There was no obvious absorption band at 747 and 1085 cm^{-1} observed at the end of experiments, indicating a limited vaterite phase produced in the urease-induced system with urease concentration between 1 and 5 g/L. This finding also corresponded to the previous XRD results. The study by Li et al. [16] on the calcium carbonate induced by carbonic anhydrase also revealed that the calcite phase was the primary formation after 24 h. Figure 5d presents that the vaterite phase was formed at 12 h in 8 g/L urease concentration. The fast precipitation rate caused by higher urease concentration might lead to the unstable reaction process which could yield the formation of vaterite. The initial precipitation of vaterite phase at very high urease activities was also reported by Van Paassen [27] and Al Qabany et al. [2].

Figures 7 and 8 show the SEM images of bacteria and urease-induced system at different precipitation times, respectively, corresponding to those of FTIR spectra. In the bacteria-induced system, the spherulitic crystals were observed at the beginning of the bacteria-induced system in all bacteria concentration, while the size of the spherulitic crystals tended to grow at 24 h. When OD_{600} = 0.1, the

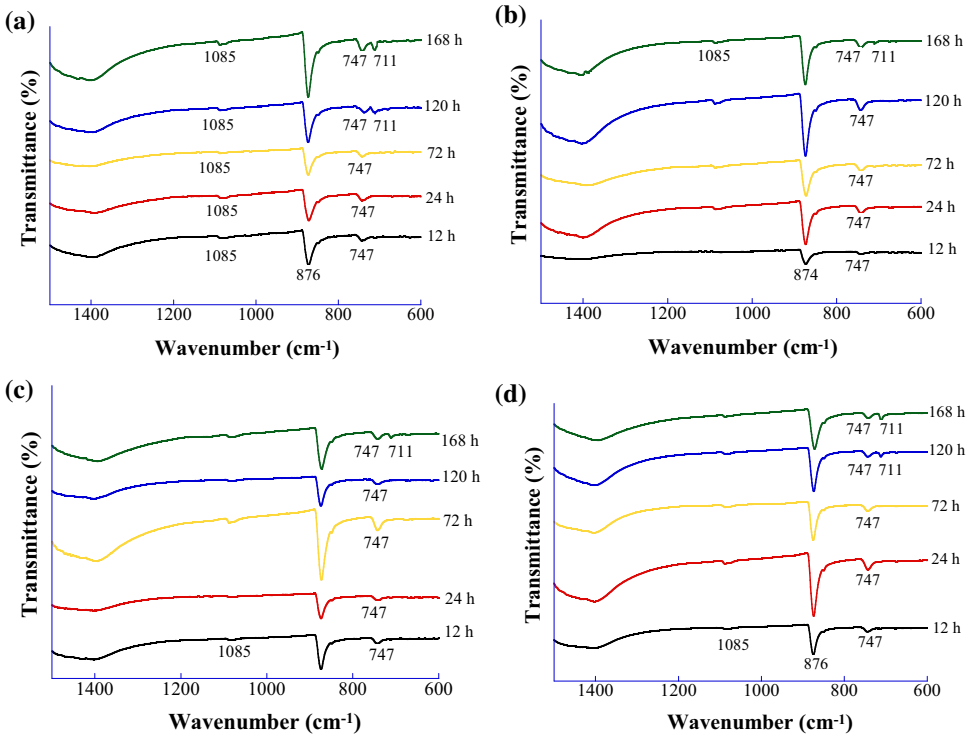

Fig. 5 FTIR spectra of $CaCO_3$ crystals as function of time at different initial bacteria concentrations. **a** OD_{600} = 0.1, **b** OD_{600} = 0.3, **c** OD_{600} = 0.6, **d** OD_{600} = 1.0

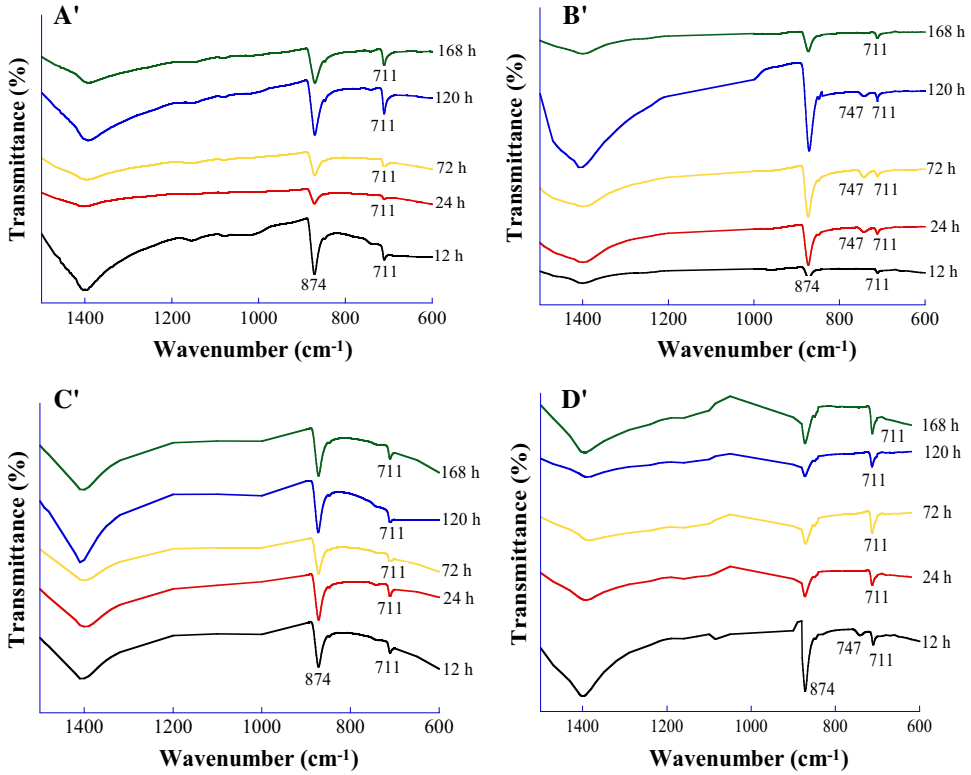

Fig. 6 FTIR spectra of $CaCO_3$ crystals as function of time at different initial urease concentrations. **a'** urease = 1.0 g/L, **b'** urease = 2.5 g/L, **c'** urease = 5.0 g/L, **d'** urease = 8.0 g/L

rhombohedral crystal started to be formed at 72 h, and the precipitates were flowerlike crystals at 168 h. The flowerlike crystals were also observed at 72 h as OD_{600} is higher than 0.3, and then the large prismatic crystals with wrinkled surface were formed at 168 h, suggesting that the crystals consisted of vaterite and calcite phase.

Overall, the comprehensive results of XRD, FTIR and SEM indicated that the vaterite phase formed at the beginning and partly transformed to calcite phase in the bacteria-induced system. Sondi and Salopek-Sondi [24] reported that sporosarcina pasteurii could produce a large amount of acidic amino acids, e.g., aspartic acid and glutamic acid, at the surface of the sporosarcina pasteurii urease. The presence of aspartic acid in solution tended to control the formation of vaterite, and higher concentrations of aspartic acid would favor the formation of vaterite [26]. The amino acids of aspartic and glutamic acid were more like a nucleus during the formation of vaterite. That is why the vaterite phase was the preferential formation in the sporosarcina pasteurii-induced system.

In the case of urease-induced system, the small prismatic crystals with wrinkled surface were observed at 12 h as urease concentration is lower than 5 g/L. There were some spherulitic crystals found in the surface of crystals at 12 h in 8 g/L urease concentration, indicating a vaterite phase formed in the beginning. This finding corresponded to FTIR results. The crystal phase did not show remarkable differences along with time in 1.0 g/L urease concentration. Some large polyhedron shape was observed along with time as urease concentration was higher than 2.5 g/L, and the spherulitic crystals disappeared with longer reaction time in 8 g/L urease concentration. Overall, the integrated results of XRD, FTIR and SEM suggest that in the urease-induced system, calcite phase was the major formation of the $CaCO_3$ crystals.

The formation of $CaCO_3$ crystals on sand particles was also studied for comparing with crystals on glass slices. The SEM images of $CaCO_3$ crystals on sand after 168 h at OD_{600} = 0.6 and 0.25 M Ca cementation media are shown in Fig. 8a. Both spherulitic and rhombohedral sharp crystal was found in the bacteria-induced system on sand surface after 168 h. Meanwhile, the flowerlike crystals were observed on sand particles as arrow indicated in Fig. 8a, which is consistent with the $CaCO_3$ crystal precipitated on glass slices. For the urease-induced system (Fig. 8b), the $CaCO_3$ crystals precipitated on sand particles were major formed in a small prismatic shape, which is similar to that on the glass slices.

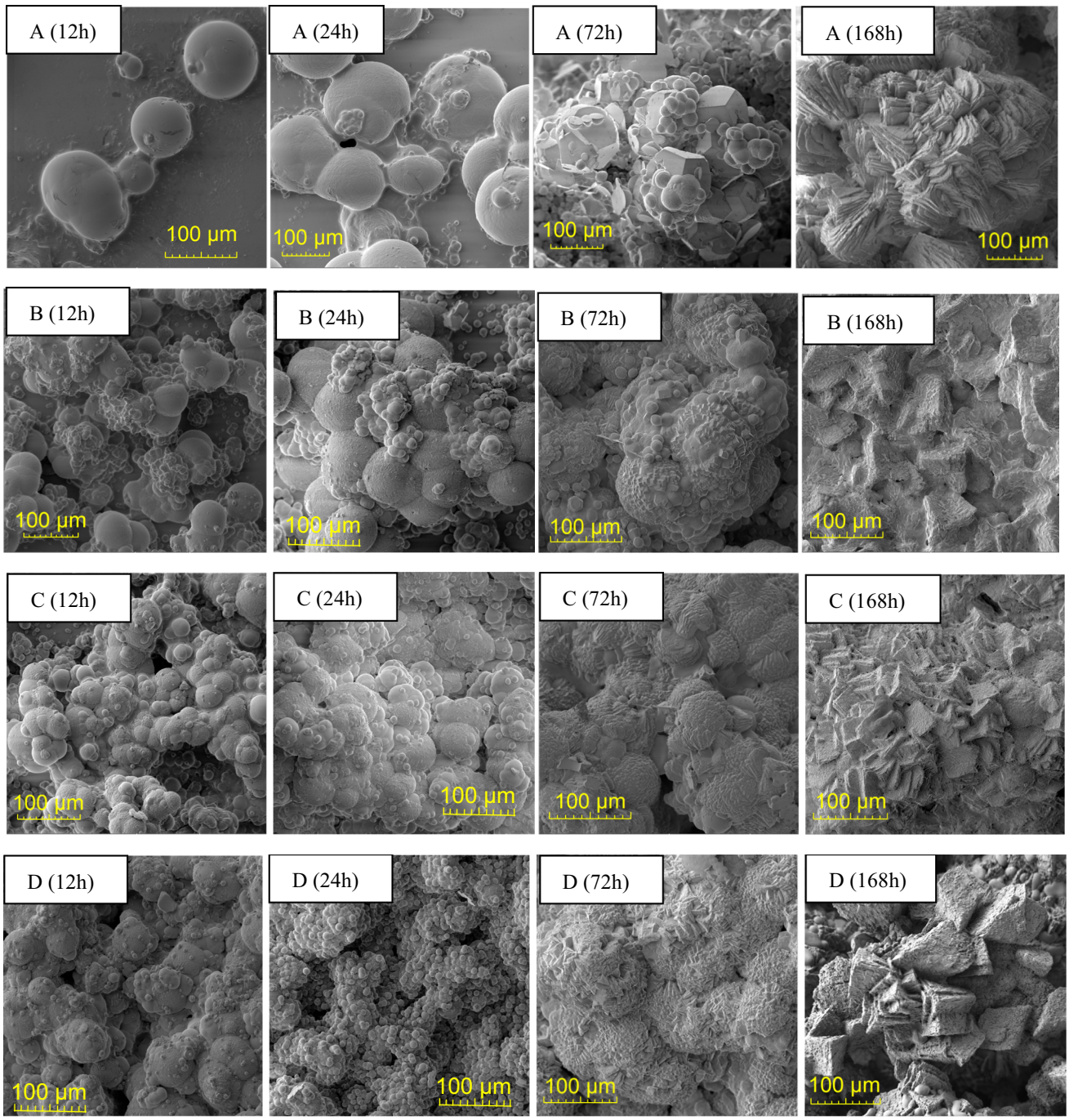

Fig. 7 SEM image of $CaCO_3$ crystal at different bacteria concentrations. **a** OD_{600} = 0.1, **b** OD_{600} = 0.3, **c** OD_{600} = 0.6, **d** OD_{600} = 1.0

4 Discussion

Bacteria-induced $CaCO_3$ crystals were sparse in 12 h as OD_{600} of 0.1, but the size of individual particles at OD_{600} of 0.1 was larger than that at urease concentration of 1.0 g/L. More crystals precipitated and united together in both scale and density along with the time. The shape of $CaCO_3$ crystals was spherulitic within the first 72 h, which may be caused by the acidic amino acids produced by bacteria. After that, the shape started to change, and the rhombohedral crystals began to form. The results from FTIR also verified that the calcite phase appeared after 72 h. The results in Fig. 1 reveal that the activities of bacteria reduced after 72 h. Also, bacteria with negative surface charge could attract the Ca^{2+} ions and then wrapped by $CaCO_3$ crystals [10]. Therefore, less acidic amino acids may be produced in solution. Sondi and Salopek-Sondi [24] reported that the vaterite phase favored a high

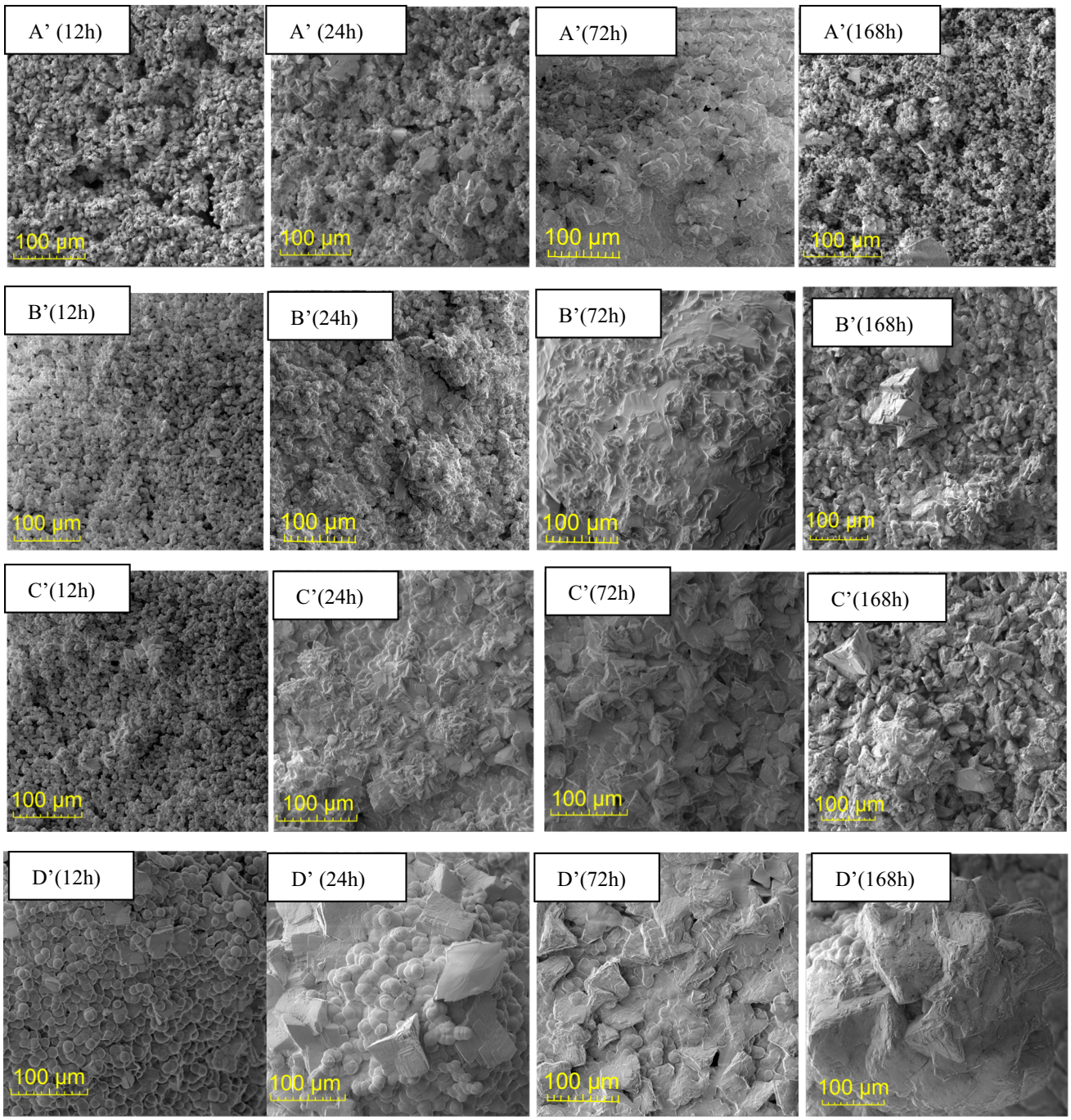

Fig. 8 SEM image of $CaCO_3$ crystal at different urease concentrations. **a'** urease = 1.0 g/L, **b'** urease = 2.5 g/L, **c'** urease = 5.0 g/L, **d'** urease = 8.0 g/L

concentration of acidic amino acids. The possible reducing concentration of acidic amino acids also explained that there were only small spherulitic crystals attached on the surface at 72 h; however, the acidic amino acids contraction test did not conducted in this paper. Meanwhile, there were no apparent spherulitic crystals on the surface at 168 h, and most of crystals were found in cubic shape. The XRD results found both vaterite and calcite at 168 h, which may indicate that the vaterite crystals undergo dissolution and recrystallization process, thus transform to calcite crystals. Li et al. [16] used bacterial carbonic anhydrase to induce $CaCO_3$ in NH_4HCO_3 and $CaCl_2$ solution. They also found that the vaterite was gradually formed in the initial stage ($\sim$ 24 h), and then no vaterite appeared at 72 h. In contrast, the crystals were smaller but more uniformly in the urease-induced system than those in the bacteria-

induced system. However, the shape and size of crystals did not have obvious changes until the urease concentration exceeded 5.0 g/L. The $CaCO_3$ crystals produced by the urease were almost in calcite phase which was confirmed by results reported by Yasuhara et al. [34].

Many researches had reported that both MICP and EICP processes can achieve a certain amount of $CaCO_3$ precipitations [7–9, 13, 22, 31, 36]. Among them, Zhao et al. [36] compared the mechanical properties of MICP-treated sand and EICP-treated sand. They found that MICP-treated samples (OD_{600} = 0.6) achieved unconfined compression strength of 1.48 MPa which was approximately four times than EICP-treated samples (5.0 g/L). From this study, the different morphologies of $CaCO_3$ crystals were found from MICP and EICP treatment, and it may explain the differences in mechanical behavior between MICP and EICP-treated samples. The bacteria-induced $CaCO_3$ tended to achieve larger crystals and may provide better bonding for larger soil particles like sand and gravel. However, the microbial growth needed aerobic environment may limit deeper applications [18]. For EICP, the $CaCO_3$ crystals were smaller and more uniform which may suit for fine particles. However, the treatment of fine particles through EICP may not go deep because the reaction time of EICP is short and the precipitated crystals will fill up the gap between particles and block the channel for further precipitation.

5 Conclusions

In this study, a series of experiments were conducted to investigate the effect of bacteria and urease concentration on the kinetics of Ca^{2+} concentration, and the morphology of $CaCO_3$ crystals obtained from MICP/EICP processes was analyzed by XRD, FTIR and SEM. The results showed that higher bacteria and urease concentration could yield the faster decrease in Ca^{2+} concentration, and the reaction ceased after 72 h in EICP processes. Meanwhile, the OD_{600} of 0.6 or urease concentrations of 5 g/L can achieve the complete reaction in MICP or EICP processes in 0.25 M cementation media. The comprehensive results of XRD, FTIR and SEM indicated that the vaterite phase was the major form of $CaCO_3$ crystals within 72 h and calcite phase was partly observed along with time in the bacteria-induced system. The vaterite phase favored the bacteria-induced solution. The integrated results of XRD, FTIR and SEM suggested that in the urease-induced system, calcite phase was the major form of the $CaCO_3$ crystals. The crystals were smaller but more uniformly in the urease-induced system than those in the bacteria-induced system.

Acknowledgements This paper is based upon work supported by the Nation Science Foundation Grant Nos. 1531382, 1924241 and U.S. Department of Transportation Grant No. (DTRT13-G-UTC50FHWA) through Maritime Transportation Research and Education Center.

References

1. Al Imran M, Shinmura M, Nakashima K, Kawasaki S (2018) Effects of various factors on carbonate particle growth using ureolytic bacteria. Mater Trans 59(9):1520–1527
2. Al Qabany A, Soga K, Santamarina C (2011) Factors affecting efficiency of microbially induced calcite precipitation. J Geotech Geoenviron 138(8):992–1001
3. Almajed A, Khodadadi H Kavazanjian Jr E (2018) Sisal fiber reinforcement of EICP-treated soil. In: IFCEE, pp 29–36
4. Almajed A, Tirkolaei HK, Kavazanjian E, Hamdan N (2019) Enzyme induced biocemented sand with high strength at low carbonate content. Sci Rep 9(1):1135
5. Bu C, Wen K, Liu S, Ogbonnaya U, Li L (2018) Development of bio-cemented constructional materials through microbial induced calcite precipitation. Mater Struct 51(1):30
6. Bu C, Wen K, Liu S, Ogbannaya U, Li L, Amini F (2018) Development of a rigid full contact mold for preparing bio-beams through microbial induced calcite precipitation. Geotech Test Method ASTM 42(3):656–669. https://doi.org/10.1520/GTJ20170148
7. Cheng L, Shahin MA, Mujah D (2016) Influence of key environmental conditions on microbially induced cementation for soil stabilization. J Geotech Geoenviron 43(1):04016083
8. Chu J, Ivanov V, Naeimi M, Stabnikov V, Liu HL (2014) Optimization of calcium-based bioclogging and biocementation of sand. Acta Geotech 9(2):277–285
9. DeJong JT, Fritzges MB, Nüsslein K (2006) Microbially induced cementation to control sand response to undrained shear. J Geotech Geoenviron 132(11):1381–1392
10. DeJong JT, Mortensen BM, Martinez BC, Nelson DC (2010) Bio-mediated soil improvement. Ecol Eng 36(2):197–210
11. Dyer M, Viganotti M (2016) Oligotrophic and eutrophic MICP treatment for silica and carbonate sands. Bioinspir Biomim Nan 6(3):168–183
12. Ghosh T, Bhaduri S, Montemagno C, Kumar A (2019) Sporosarcina pasteurii can form nanoscale calcium carbonate crystals on cell surface. PLoS ONE 14(1):e0210339
13. Hamdan N, Kavazanjian Jr E, O'Donnell S (2013) Carbonate cementation via plant derived urease. In: Proceedings of the 18th international conference on soil mechanics and geotechnical engineering, Paris
14. Kavazanjian E Jr, Almajed A, Hamdan N (2017) Bio-inspired soil improvement using EICP soil columns and soil nails. Grouting 2017:13–22
15. Li W, Liu L, Chen W, Yu L, Li W, Yu H (2010) Calcium carbonate precipitation and crystal morphology induced by microbial carbonic anhydrase and other biological factors. Process Biochem 45(6):1017–1021
16. Li W, Chen WS, Zhou PP, Zhu SL, Yu LJ (2013) Influence of initial calcium ion concentration on the precipitation and crystal morphology of calcium carbonate induced by bacterial carbonic anhydrase. Chem Eng J 218:65–72
17. Li M, Li L, Ogbonnaya U, Wen K, Tian A, Amini F (2015) Influence of fiber addition on mechanical properties of MICP-treated sand. J Mater Civ Eng 28(4):04015166
18. Li M, Wen K, Li Y, Zhu L (2018) Impact of oxygen availability on microbially induced calcite precipitation (MICP) treatment. Geomicrobiol J 35(1):15–22

19. Lin H, Suleiman MT, Brown DG, Kavazanjian E Jr (2015) Mechanical behavior of sands treated by microbially induced carbonate precipitation. J Geotech Geoenviron 142(2):04015066
20. Loste E, Wilson RM, Seshadri R, Meldrum FC (2003) The role of magnesium in stabilising amorphous calcium carbonate and controlling calcite morphologies. J Cryst Growth 254(1–2):206–218
21. Manoli F, Dalas E (2000) Spontaneous precipitation of calcium carbonate in the presence of chondroitin sulfate. J Cryst Growth 217(4):416–421
22. Martinez BC, DeJong JT, Ginn TR, Montoya BM, Barkouki TH, Hunt C et al (2013) Experimental optimization of microbial-induced carbonate precipitation for soil improvement. J Geotech Geoenviron 139(4):587–598
23. Mortensen BM, Haber MJ, DeJong JT, Caslake LF, Nelson DC (2011) Effects of environmental factors on microbial induced calcium carbonate precipitation. J Appl Microbiol 111(2):338–349
24. Sondi I, Salopek-Sondi B (2005) Influence of the primary structure of enzymes on the formation of $CaCO_3$ polymorphs: a comparison of plant (*Canavalia ensiformis*) and bacterial (*Bacillus pasteurii*) ureases. Langmuir 21(19):8876–8882
25. Stocks-Fischer S, Galinat JK, Bang SS (1999) Microbiological precipitation of $CaCO_3$. Soil Biol Biochem 31(11):1563–1571
26. Tong H, Ma W, Wang L, Wan P, Hu J, Cao L (2004) Control over the crystal phase, shape, size and aggregation of calcium carbonate via a L-aspartic acid inducing process. Biomaterials 25(17):3923–3929
27. Van Paassen LA (2009) Biogrout, ground improvement by microbial induced carbonate precipitation, Doctoral dissertation, TU Delft, Delft University of Technology
28. Wang Y, Soga K, Dejong JT, Kabla AJ (2019) A microfluidic chip and its use in characterising the particle-scale behaviour of microbial-induced calcium carbonate precipitation (MICP). Géotechnique 69(12):1–9
29. Wen K, Bu C, Liu S, Li Y, Li L (2018) Experimental investigation of flexure resistance performance of bio-beams reinforced with discrete randomly distributed fiber and bamboo. Constr Build Mater 176:241–249
30. Wen K, Li Y, Liu S, Bu C, Li L (2019) Development of an improved immersing method to enhance microbial induced calcite precipitation treated sandy soil through multiple treatments in low cementation media concentration. Geotech Geol Eng 37(2):1015–1027
31. Wen K, Li Y, Liu S, Bu C, Li L (2019) Evaluation of MICP treatment through electric conductivity and pH test in urea hydrolyzed process. Environ Geotech. https://doi.org/10.1680/jenge.17.00108
32. Xu X, Han JT, Cho K (2004) Formation of amorphous calcium carbonate thin films and their role in biomineralization. Chem Mater 16(9):1740–1746
33. Yasuhara H, Hayashi K, Okamura M (2011) Evolution in mechanical and hydraulic properties of calcite-cemented sand mediated by biocatalyst. In: Geo-frontiers 2011: advances in geotechnical engineering, pp 3984–3992
34. Yasuhara H, Neupane D, Hayashi K, Okamura M (2012) Experiments and predictions of physical properties of sand cemented by enzymatically-induced carbonate precipitation. Soils Found 52(3):539–549
35. Zhang Y, Guo HX, Cheng XH (2015) Role of calcium sources in the strength and microstructure of microbial mortar. Constr Build Mater 77:160–167
36. Zhao Q, Li L, Li C, Li M, Amini F, Zhang H (2014) Factors affecting improvement of engineering properties of MICP-treated soil catalyzed by bacteria and urease. J Mater Civ Eng 26(12):04014094